Identifying Spurious Correlations using Counterfactual Alignment

Anonymous authors
Paper under double-blind review

Abstract

Models driven by spurious correlations often yield poor generalization performance. We propose the counterfactual (CF) alignment method to detect and quantify spurious correlations of black box classifiers. Our methodology is based on counterfactual images generated with respect to one classifier being input into other classifiers to see if they also induce changes in the outputs of these classifiers. The relationship between these responses can be quantified and used to identify specific instances where a spurious correlation exists. This is validated by observing intuitive trends in a face-attribute face-attribute and waterbird classifiers, as well as by fabricating spurious correlations and detecting their presence, both visually and quantitatively. Furthermore, utilizing the CF alignment method, we demonstrate that we can evaluate robust optimization methods (GroupDRO, JTT, and FLAC) by detecting a reduction in spurious correlations.

1 Introduction

Challenges related to neural network generalization and fairness often arise due to covariate shift (Moreno-Torres et al., 2012) and shortcut learning (Ross et al., 2017; Geirhos et al., 2020). Shortcut learning can lead to models making decisions based on factors not aligned with expectations of the model creator. These powerful models (vision models in this work) leverage a wide array of features and relationships, which may inadvertently incorporate unwanted spurious correlations. These spurious relationships may stem from sample bias (e.g., predicting cows when cows are observed on grass but not on a beach) or may be inherent to the class definition (e.g., predicting cows when an animal has four legs) (Beery et al., 2018).

In this work our objective is to understand black-box classifiers, without access to their training data, as this is a common use case encountered by practitioners. In this analysis, we utilize counterfactual (CF) images which are synthetic images simulating a change in the class label of an image (Pearl, 2009). These synthetic images have features modified such that the prediction of the classifier changes. We can then view the synthetic images to understand the reasons that a prediction was made.

Specifically, we are interested in CF images that are directly generated using the gradients of a classifier (Cohen et al., 2021; Joshi et al., 2018; Balasubramanian et al., 2020). Generating CF images with respect to a classifier is rooted in similar logic to that of crafting adversarial examples. However, the key distinction lies in the constraint that CF images remain within the data manifold of plausible images. The latent space of an autoencoder provides such data manifold. This approach enables us to study the specific features used by a given classifier on a particular input. By keeping the classifier and autoencoder independent, different classifiers can be analysed using a singular fixed autoencoder as a reference point.

The task of interpreting these CF images presents new challenges of scale. Spurious correlations may only exist in a handful of samples where rare features occur together. Locating these samples requires investigating the features used for each prediction, which can be automated using the approaches we present in this study.

The approach we take is to generate CF images for the positive predictions of a classifier over an entire dataset and study the resulting CF images using a collection of different classifiers, which we refer to as downstream classifiers, to observe what outputs are impacted. If the CF images generated for one classifier

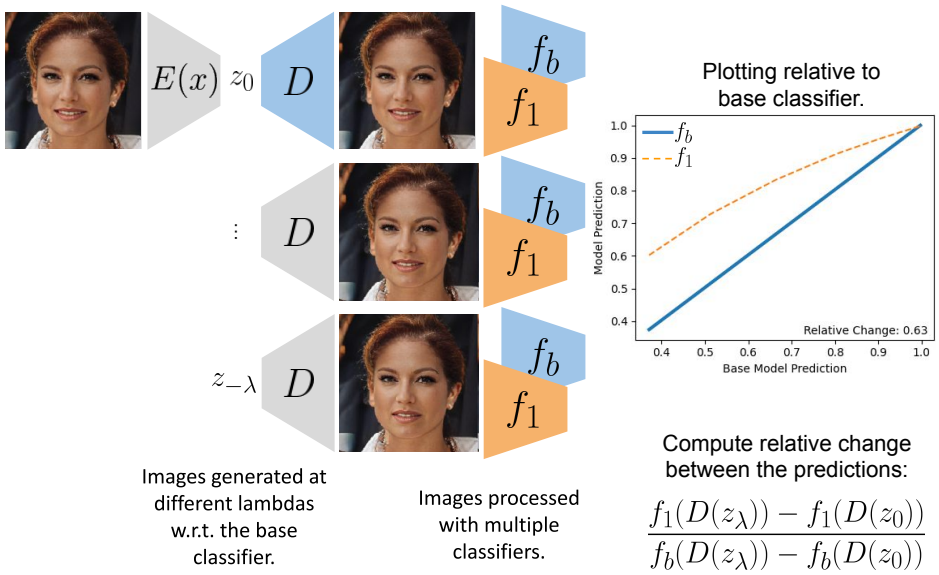

Figure 1: Overview of the alignment methodology. An image is encoded, reconstructed, and then processed by a classifier. The counterfactual is generated by subtracting the gradient of the classifier output w.r.t. the latent representation. The resulting representation is reconstructed back into an image. The reconstructed images are processed with multiple classifiers and the classifier outputs can be plotted side by side to study their alignment. The base model value can be used as the x-axis to more easily compare it to the predictions of another classifier. The output changes can be quantified and compared using relative change.

also change the predictions of other classifiers, we can conclude that there is shared feature usage. This shared feature usage can prompt us to investigate unexpected relationships. The relative change metric (Eq. 3) can be used to quantify the impact of counterfactual perturbations and identify spurious correlations that may occur for a specific example or to identify trends across an entire dataset. We study face-attribute classification, recognizing its advantage in allowing visual verification by readers.

Overall, given the problem setting of spurious correlations, the contributions of this work include:

- We propose CF alignment to reason about the feature relationships between classifiers, quantified using the relative change metric. This approach allows for both aggregate quantification and targeted querying of models to locate specific examples where the spurious correlations are used to make predictions.
- Our work demonstrates the ability to detect spurious correlations on existing face-attribute and waterbird classifiers. This is validated by observing intuitive trends in a face-attribute classifier as well as inducing spurious correlations and then detecting their presence, both visually and quantitatively.
- We demonstrate that CF Alignment can evaluate robust optimization methods (GroupDRO, JTT, and FLAC) by detecting a reduction in spurious correlations. We also observe improved generalization performance when a spurious correlation is reduced.

2 Related Work

Counterfactual (CF) generation can be done in a variety of ways (Verma et al., 2020). Classifier specific approaches generally perturb a latent space representation guided by a classifier. Some methods use the gradient of a classifier to guide movement in the latent space by computing the gradient directly (Cohen et al., 2021) or defining a loss that is optimized (Joshi et al., 2018; Balasubramanian et al., 2020). Another classifier based approach is to train a model that predicts, using training examples, where to walk in the

latent space to change the classifier's prediction (Schutte et al., 2020). This has the benefit of working with classifiers that are not differentiable. Another approach is conditional generation which doesn't use a classifier and instead generates images based on a conditioning variable. This conditioning can be a label (Mirza & Osindero, 2014; Baumgartner et al., 2018; Samangouei et al., 2018; Schutte et al., 2020; Hasenstab et al., 2023; Barredo-Arrieta & Del Ser, 2020; Singla et al., 2023) or text (Chambon et al., 2022), or can be provided by manually adjusting the latent representation (Seah et al., 2019). Conditional generation learns a representation from the data and does not capture the exact features utilized by a classifier, as the gradient based methods do.

Several methods exist for studying neural network based classifiers to understand the features they use. Early approaches include gradient based attribute maps (aka saliency heatmaps) that could be overlaid on the image (Simonyan et al., 2014). This was extended to capture more caveats of neural network reasoning (Sundararajan et al., 2017; Springenberg et al., 2015) but these methods still only generate heatmap explanations. Other work focuses on leveraging occlusions to identify discrete image regions (Ribeiro et al., 2016) that are relevant to a prediction. This is useful when predictions are based on discrete features that are smaller than the occlusion size. Other work inspects individual neural network neurons to identify where class information is propagating using linear probing (Alain & Bengio, 2016) and manual identification (Olah et al., 2020; 2017). This is useful for understanding the internal representations of neural networks but does not explain individual predictions.

Along these lines, work by Kim et al. (2018) focuses on concepts represented by layer activations forming so called "Concept Activation Vectors". These vectors allow us to identify inputs which result in a similar internal state and therefore have a similar reason for being predicted. A limitation of this approach is that it is difficult to compare vectors between classifiers because they have different weights.

An approach by Balakrishnan et al. (2021) generates synthetic images using human annotators such that the images have known feature similarity (e.g. a face with all features held constant except for skin color). These images can then be used to identify spurious correlations between attributes. To contrast this approach to ours, this work is creating CFs manually using humans and then looking for unexpected changes in classifier predictions, similar to our approach. A limitation of this method is the required manual effort and the reliance on human knowledge of concepts. The automatic generation of CFs in our work overcomes this issue and allows us to identify features that are unknown initially to humans. And the relative change metric makes it easy to identify potential spurious correlations.

3 CF Alignment Methodology

In this work, we introduce the CF alignment approach, outlined in Figure 1. The methodology involves the generation of counterfactual samples using a technique known as Latent Shift (Cohen et al., 2021). The implementation of Latent Shift requires the integration of an encoder/decoder model, denoted as $D(E(x))$, where E represents the encoder and D is the decoder. Additionally, a classifier f is incorporated, responsible for predicting the target variable y, expressed as $y = f(x)$. It is important to note that both the autoencoder and the classifier are trained independently, with the only specified requirements being differentiability and operation on the same data domain.

To compute a counterfactual, the process begins with encoding an input image x using the encoder $E(x)$, resulting in a latent representation z. The next step involves perturbing the latent space to generate counterfactual samples. This perturbation is performed using a base classifier f_b, as illustrated in Equation 1. The resulting perturbed latent representation is denoted as z_λ. Subsequently, the decoder D is employed to reconstruct the image, resulting in a counterfactual image x'_λ, as depicted in Equation 2.

The perturbation of the latent space, represented by z_λ, is computed by subtracting λ times the gradient of the base classifier f_b with respect to the latent representation z. This operation is conducted to induce changes in the latent space that influence the predictions of the classifier. The parameter λ is determined through an iterative search process, where its value is systematically adjusted in steps. The objective is to find a suitable λ such that the classifier's prediction is either reduced by 0.6 or starts to increase. 0.6 is

chosen as a difference that should cross the decision boundary. Just crossing the 0.5 mark is not always large enough to generate a reasonable counterfactual.

$$z_\lambda = z_0 - \lambda \frac{\partial f_b(D(z_0))}{\partial z} \tag{1}$$

$$x'_\lambda = D(z_\lambda) \tag{2}$$

Equation 1 expresses the computation of z_λ, and Equation 2 outlines the generation of the counterfactual image x'_λ by decoding the perturbed latent representation.

This process allows us to systematically explore and manipulate the latent space to generate counterfactual samples that reveal insights into the decision-making process of the classifier and its sensitivity to changes in the input data.

3.1 Relative Change

Having generated counterfactual samples using the Latent Shift approach, we proceed to algorithmically assess the impact of these samples on various downstream classifiers responsible for predicting the probability of different attributes, denoted as f_1, f_2, and so on. These classifiers are distinct from the base classifier, denoted as f_b, which was utilized in the counterfactual generation process.

To quantify the relationship between the base classifier and each downstream classifier, we employ the "relative change metric", as defined in Equation 3. This metric is akin to correlation but takes into account not only the direction of change in predictions but also the magnitude of that change. The formula for relative change is expressed as follows:

$$R(f_1, f_b, z_0) = \frac{f_1(D(z_\lambda)) - f_1(D(z_0))}{f_b(D(z_\lambda)) - f_b(D(z_0))} \tag{3}$$

Here, $D(z_\lambda)$ and $D(z_0)$ represent the reconstructions of the latent representations z_λ and z_0 (perturbed and original, respectively) by the decoder D. The numerator captures the change in prediction made by the downstream classifier f_1 in response to the counterfactual perturbation, while the denominator corresponds to the change in prediction made by the base classifier f_b due to the same perturbation.

In our experiments, we opted for relative change over traditional correlation measures. This decision was motivated by the observation that correlation metrics occasionally yielded false positives when only a slight change in the prediction of f_1 occurred compared to the base classifier f_b. Relative change provides a more nuanced understanding by considering not just the direction but also the magnitude of the change, offering a more robust assessment of the impact of counterfactual perturbations on downstream classifiers.

The relative change metric is a key contribution that allows us to make sense of the CF alignment results at scale over large datasets.

4 Experiments

The experiments in this work are performed on the CelebA HQ dataset (Karras et al., 2018) that contains over 200k celebrity images with 40 facial attribute labels per image. The resolution of the images is 1024×1024. Experiments are also performed on the lower resolution (178 x 178) CelebA dataset (Liu et al., 2015).

The pre-trained face classifiers used in this work are sourced from (Vandenhende et al., 2020). They were trained on the CelebA dataset (Liu et al., 2015) to predict 40 different facial attributes on images of dimensions 224×224. We chose this model because it has good performance, is publicly available, and was implemented in PyTorch.

We leverage the VQ-GAN autoencoder from (Esser et al., 2021) trained on the FacesHQ dataset, which combines the CelebA HQ dataset (Karras et al., 2018) and the Flickr-Faces-HQ (FFHQ) dataset (Karras et al., 2021). The resolution of this model is 256x256. In order to make this work for existing classifiers, each classifier normalizes the input image dynamically to match its training domain.

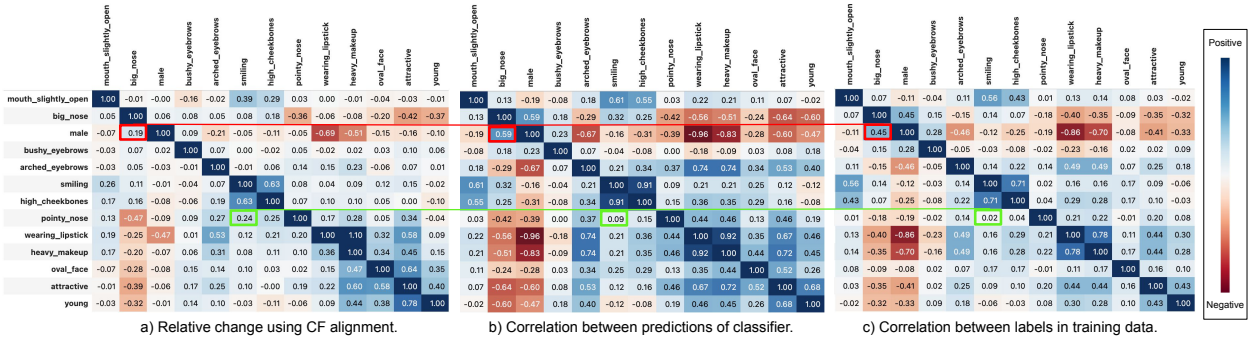

a) Relative change using CF alignment. b) Correlation between predictions of classifier. c) Correlation between labels in training data.

Figure 2: Relationships between face-attribute classifiers as measured by CF-alignment relative changes (left), classifier predictions (middle) and training data labels (right). In (a), base classifiers are along the rows and downstream classifiers are along the columns. Comparing (a) to (b) and (c), shows that many relationships reflected in the CF outputs are preserved from correlations in the training data. We draw the readers attention to some unique differences. The relationship between *male* and *big_nose*, highlighted in red, is strong in both the classifier predictions and ground truth labels but low in CF alignment, indicating that although correlated, these features are not exploited by the classifier. In contrast to this, the relationship between *pointy_nose* and *smiling*, highlighted in green, is weak in both the classifier predictions and ground truth labels but high in CF alignment, indicating that this relationship was introduced by the classifier.

The Captum library (Kokhlikyan et al., 2020) is utilized for baseline attribution methods. PyTorch (Paszke et al., 2019) is used for efficient tensor computation and automatic differentiation. The source code and model weights for all experiments will be released publicly online*. The CF alignment algorithm requires a few seconds to run for each image on a NVIDIA V100 16GB GPU. The CF generation step is the most expensive and is variable due to the automated search for the optimal lambda. The resulting CF images are then processed by each classifier which scales by the number of classifiers studied.

4.1 Aggregate statistics over a dataset

Viewing aggregate CF alignment statistics over a dataset can be useful when investigating a model for bias or spurious correlations. The average relative change between pairs of classifiers (N=400 per class) is shown in Figure 2a. Figures 2b and 2c show correlations between classifier predictions and the ground truth training labels. A subset of classifiers studied are shown in this figure for clarity, with the full CF alignment matrix in Appendix Fig. 7. These classifiers were chosen because they have intuitive and unintuitive relationships with large relative change that help to illustrate the contribution of this method.

The caption of Figure 2 details observations where correlation in the training data and classifier outputs are not the same as the relationships uncovered using CF alignment. These indicate that even if correlated attributes are presented to the classifier it does not cause feature usage to be correlated. These observations also imply that even if uncorrelated attributes are presented to the classifier it may still construct spurious feature relationships.

4.2 Studying specific examples

Using the aggregate analysis from §4.1 as a guide, classifiers can be selected to investigate undesired relationships on specific images. Inspecting the *pointy_nose* classifier in Figure 3 using two images with positive predictions for *pointy_nose* we observe similar and contrasting relationships between classifiers. A common theme is the inverse alignment with *big_nose* which is intuitive as it is the opposite of a pointy nose. *rosy_cheeks* is a common aligned classifier which does not appear to have an obvious reason and is likely a spurious correlation. An alignment with *smiling* is only observed in one of the examples.

*BLINDED

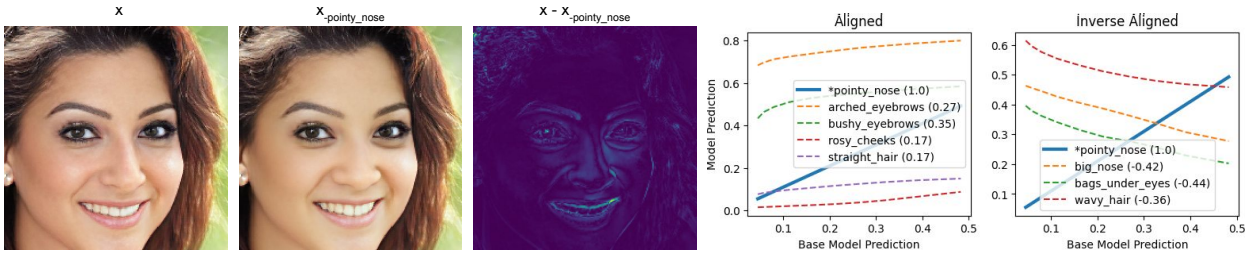

(a)

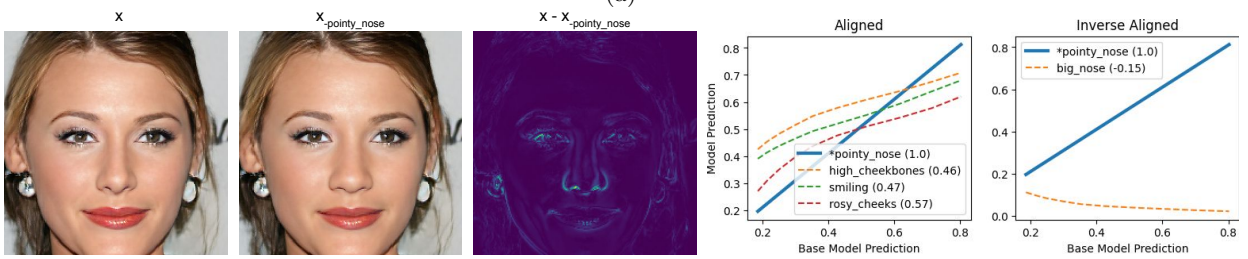

(b)

Figure 3: CF alignment examples for *pointy_nose* with the highest aligned and inverse aligned classifiers. We observe an inverse alignment with *big_nose* and potential spurious relationships with eyebrows, eyes, hair, and smiling. The relative change is shown next to each classifier name.

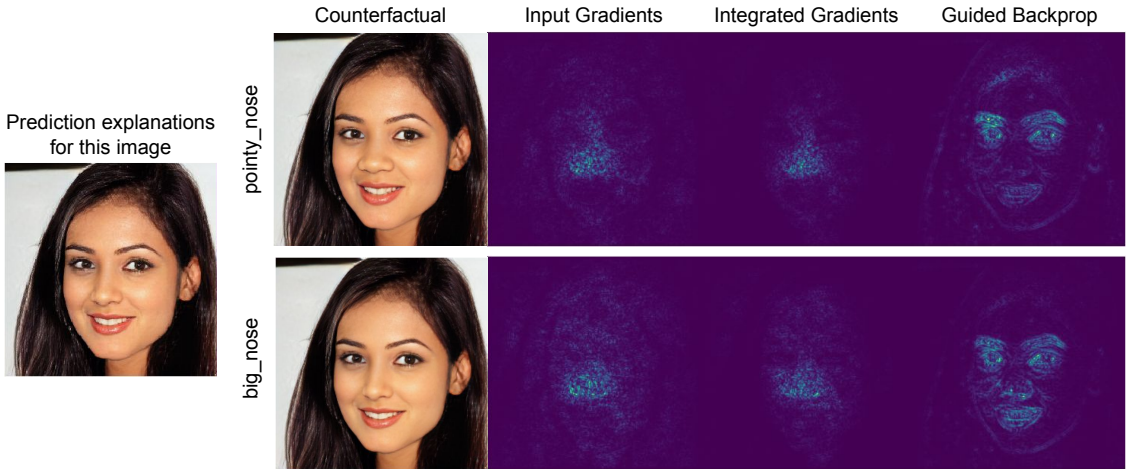

Figure 4: Example of saliency maps failing to provide meaningful localization when the concepts overlap with each other. Here, saliency map methods localize around the nose which doesn't provide the ability to distinguish between a big or pointy nose prediction.

A takeaway from these examples is the uniqueness of a spurious correlations to specific images with specific features, thus demonstrating the need for the method we present to mine for examples where these spurious correlations can be observed.

4.3 Comparison with saliency maps

Saliency maps for feature attribution could potentially be used to perform a similar analysis by looking at relationships between their generated heatmaps. Here, we present an example that demonstrates their limitation. The attribution methods input gradients, integrated gradients Sundararajan et al. (2017), and

guided backprop Springenberg et al. (2015) are used to explain the classifier predictions of *pointy_nose* and *big_nose*.

In Fig. 4 the salient areas for *pointy_nose* and *big_nose* are the same and cannot be disambiguated. The saliency maps only present information as pixel importance which overlaps because both classifiers use features on the nose. Due to these very similar heatmaps, comparing them would not allow us to conclude that the classifiers are using different features. We observe in Fig. 2 that these two classifiers have an inverse relationship. Using CF alignment, we can gain a deeper understanding of what features the model is using, and we can better reason about why the decision was made.

4.4 Validation by inducing spurious correlations

In order to further verify the CF alignment approach, we construct a classifier with a known spurious correlation and then demonstrate that this bias is observable in the CF alignment plot. A spurious correlation can be induced in the classifier by composing classifiers:

$$f_{biased}(x) = f_{smiling}(x) + 0.3 f_{arched_eyebrows}(x) \tag{4}$$

The CF alignment plot for the base *smiling* classifier predictions in Fig. 5a show that arched_eyebrows does not change and we can confirm this in the CF image. The resulting biased classifier can be observed using the *arched_eyebrows* features in Fig. 5b both visually as well as in the CF alignment plot. The CF alignment plot shows that the prediction of *arched_eyebrows* now changes and is aligned with *smiling*.

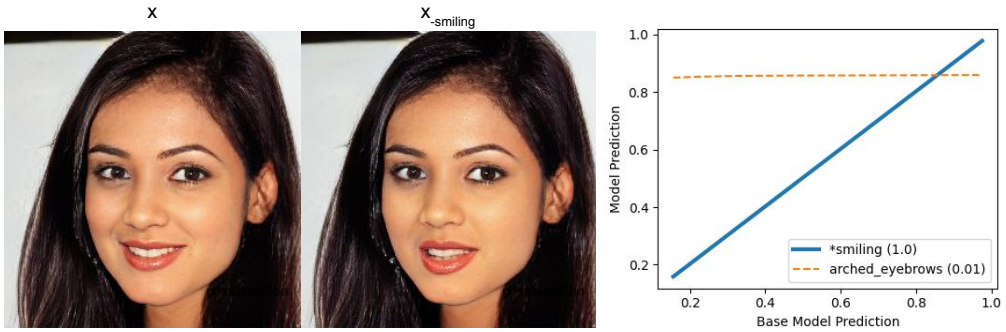

(a) CF for the classifier *smiling* showing eyebrows are unchanged. The horizontal line indicates the prediction of *arched_eyebrows* is not influenced by the features used for *smiling* in this image.

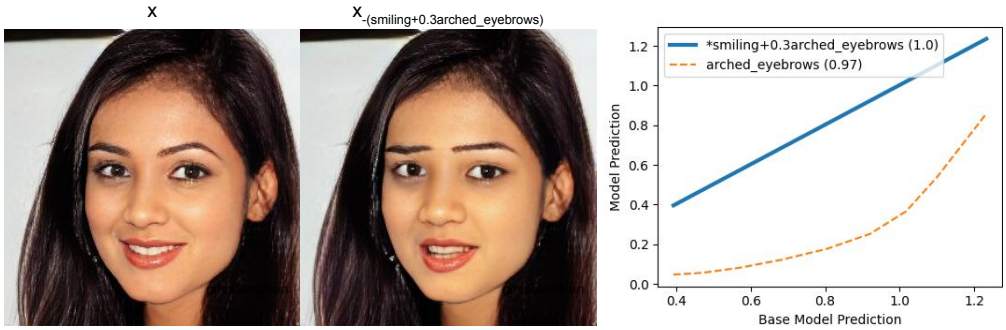

(b) CF for a modified *smiling* classifier which has been combined with an *arched_eyebrows* classifier.

Figure 5: Example of detecting a spurious correlation in a biased classifier. The classifier is biased with arched eyebrows and this is observed in the alignment plot as well as in the counterfactual image. The relative change is now 0.97 compared to 0.01 for the unchanged *smiling* classifier.

4.5 Analysis of robust optimization methods

An application of CF alignment is to assess the effectiveness of bias mitigation techniques. Various biased training settings have been developed to induce spurious correlations with sensitive attributes in models and then employ bias mitigation strategies to counter them. The experiments we present are designed to demonstrate that measuring the CF alignment with sensitive attributes can measure the impact of these methods.

To properly compare these methods, experiments are grouped based on the specific training configuration used so each baseline is unique to that setting. For this reason, these models cannot be compared side by side for the same dataset.

The bias mitigation methods we use are selected because their authors make their code available to generate pre-trained models that can be studied post-hoc. Using only pre-trained models further demonstrates the utility of our proposed approach where our method is versatile enough to evaluate these existing pre-trained models.

Experiments in this section are performed on the held out test datasets and selected to be balanced such that there is a balanced distribution of positive and negative examples with the sensitive attribute (e.g. in the CelebA dataset, 1/4 of the samples are labeled to have Blond Hair and be Male, 1/4 Blond Hair and be Not Male, 1/4 Not Blond Hair and be Not Male, and 1/4 Not Blond Hair and be Male).

During classification experiments, the samples evaluated are selected to be inversely correlated with the sensitive attribute to cause the most discrepancy in performance (e.g. Samples are selected that are labeled Blond Hair and Male as well as Not Blond Hair and Not Male).

4.5.1 GroupDRO on Waterbirds

Work on GroupDRO Sagawa et al. (2020) constructed the Waterbirds task such that there is a spurious correlation between birds (from the CUB dataset (Wah et al., 2011)) with backgrounds that contain water or land.

Three models are evaluated for this experiment, a baseline model which was induced to rely on spurious correlations, a model trained with Group Distributionally Robust Optimization (DRO) (Sagawa et al., 2020) which aims to minimize error over groups (which are known during training, in this case the background class), a model using Just Train Twice (JTT) (Liu et al., 2021) which uses a two stage approach that boosts misclassified training examples in a second training cycle. The classifiers that these models are aligned with are trained to predict if the background of an image is land or water using the same training dataset labels from the Waterbirds dataset.

A limitation of this analysis is the limited latent variable model used (A VQ-GAN trained on Open Images (Krasin et al., 2017)) that has difficulty modulating features (likely because its training domain is broad). A model that is better at representing birds would be able to generate better counterfactuals that are easier to interpret.

In Figure 6 two models are evaluated on the same image illustrating a difference in CF alignment results to a classifier that predicts the background. The relative change with the background classifier is much higher for the baseline model than the model trained with DRO (0.35 vs 0.25) indicating that training with GroupDRO prevented the models reliance on features associated with the background classifier. A magnified view of the counterfactuals of the bird's head indicate nostril size being reduced and colors becoming brighter in the model trained with DRO. This may indicate larger nostril sizes are associated with water birds which aligns with the family of waterbirds, Procellariiformes, having an enlarged nasal gland at the base of the beak for secreting salt water (Ehrlich et al., 1988). While the mallard in the image is not a Procellariiforme, nostril size may be a feature used by the classifier in general as many in the waterbirds are seabirds.

Aggregate results over 4097 samples from the test set of the waterbirds dataset reveals a reduction in mean relative change using DRO shown in Table 1. This indicates that the features used by the baseline classifier

overlap the land and water classifier and these spurious correlations were reduced when utilizing DRO. We observe that this improved model, with a lower relative change, achieves a higher classification accuracy.

(a) Evaluating a baseline model trained that is expected to use spurious correlations.

(b) Evaluating a model trained using Distributionally Robust Optimization (DRO) to reduce the spurious correlation with the background.

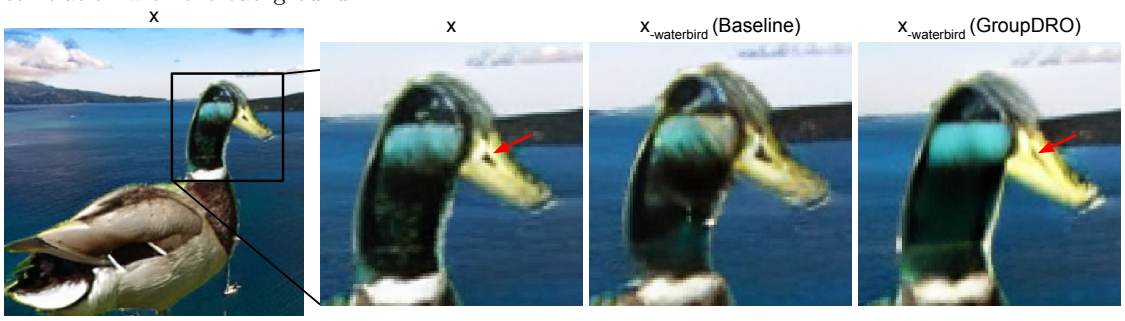

(c) A magnified view of the birds head which shows differences in nostril size and head color.

Figure 6: Counterfactuals generated for models trained on the waterbirds dataset together with CF alignment plots. (a) and (b) The relative change between the waterbird classifier and the background classifier is shown in the lower right of the plot. (c) The nostril size is reduced in the counterfactual for the DRO model indicating that a larger nostril size is associated with waterbirds.

Target	Relative change ↓ w/water classifier	Relative change ↓ w/land classifier	Classification ↑ AUC
Waterbird (baseline)	0.35±0.02	-0.36±0.03	0.69
Waterbird (groupdro)	**0.25±0.00**	**-0.22±0.03**	**0.92**
Waterbird (jtt)	0.42±0.03	-0.43±0.00	0.65

Table 1: Aggregate relative change metrics for models trained on the waterbirds test dataset (N=4097). A reduction in relative change with the land and water background classifiers indicates DRO has reduced the spurious correlation.

4.5.2 GroupDRO on CelebA

GroupDRO models are also evaluated on the CelebA dataset on the task of Blond_Hair and the sensitive attribute Male. JTT is not evaluated on this task because we were unable to generate pre-trained weights using the provided code due to memory issues that we were unable to resolve.

In Table 2 we can see the relationship between Blond_Hair and Male is negative in the baseline and then is reduced by the GroupDRO training and becomes slightly positive. This reduction results in a higher classification accuracy on the CelebA test set.

Target	Relative change ↓ w/male classifier	Classification ↑ AUC
Blond_Hair (baseline)	-0.052±0.01	0.91
Blond_Hair (groupdro)	**0.025±0.00**	**0.95**

Table 2: Methods evaluated on models that predict Blond_Hair trained on the CelebA dataset. Evaluations are performed on 1024 samples from the test set.

4.5.3 FLAC on CelebA

The work Fairness-Aware Representation Learning by Suppressing Attribute-Class Associations (FLAC) (Sarridis et al., 2023) uses pairwise similarity between the between the model representation and the representation of a bias-capturing classifier that predicts the sensitive attribute. The bias capturing classifier acts as a proxy for labels and provides embeddings that can be used to regularize the feature space of the classifier we are training. Their approach is to minimize the difference, in feature space, between samples with different sensitive attributes and the same target label as well as increase the difference between samples with the same sensitive attributes and the different target label. In Table 3 the relative change is shown to be reduced and the classification performance improves.

Target	Alpha	Relative change ↓ w/male classifier	Classification ↑ AUC
Blond_Hair	0	-0.081±0.016	0.77
Blond_Hair	30000	**-0.039±0.009**	**0.93**
Blond_Hair	60000	-0.051±0.010	0.92

Table 3: Aggregate relative change of models trained with FLAC on 1024 samples from the CelebA test set. The strength of this regularization is controlled with an α parameter.

5 Limitations

There are limitations and challenges to CF generation Verma et al. (2020) where bias can also exist in the CF generation method. Furthermore, although we are optimistic that our method will generalize to additional domains, we focus our current analysis on face-attribute classification. Although we do not demonstrate the generalizability of our method to additional domains, using face-attribute classification is a deliberate choice enabling qualitative evaluation, in addition to our quantitative evaluation. Additionally, since CF generation relies on a separate autoencoder, improving the representational capability of the autoencoder may improve the fidelity of the CF generation.

6 Conclusion

In this work we propose counterfactual (CF) alignment along with the relative change metric §3. We demonstrate that this method enables us to reason about the feature relationships between classifiers in aggregate

and to locate specific examples where the spurious correlations are used. These claims are supported with an analysis of face-attribute classifiers that identify expected and unexpected spurious correlations.

We observe that if correlated attributes are presented to the classifier, this does not cause feature usage to be correlated §4.1. We also observe that if uncorrelated attributes are presented to the classifier, the classifier may still construct spurious feature relationships.

The validity of the CF alignment method is confirmed by inducing and quantifying spurious correlations via additive composition §4.4. Classifiers are composed together to create a classifier with a known spurious correlation and then this is observed using CF alignment.

We then explore classifiers trained using robust optimization methods to demonstrate the applicability to black box classifiers and to provide more visibility into what these methods achieve §4.5.

Overall, the proposed approach may serve as an end-to-end or human-in-the-loop system to automatically detect, quantify, and correct spurious correlations for image classification tasks that lead to biased classifier outputs.

References

Guillaume Alain and Yoshua Bengio. Understanding intermediate layers using linear classifier probes. *International Conference on Learning Representations*, 2016. URL https://arxiv.org/abs/1610.01644.

Guha Balakrishnan, Yuanjun Xiong, Wei Xia, and Pietro Perona. Towards Causal Benchmarking of Bias in Face Analysis Algorithms. In *Computer Vision and Pattern Recognition*, 2021. URL http://arxiv.org/abs/2007.06570.

Rachana Balasubramanian, Samuel Sharpe, Brian Barr, Jason Wittenbach, and C. Bayan Bruss. Latent-CF: A Simple Baseline for Reverse Counterfactual Explanations. In *Neural Information Processing Systems (NeurIPS) Fair AI in Finance Workshop*, 2020. doi: 10.48550/arxiv.2012.09301. URL https://arxiv.org/abs/2012.09301.

Alejandro Barredo-Arrieta and Javier Del Ser. Plausible Counterfactuals: Auditing Deep Learning Classifiers with Realistic Adversarial Examples. In *International Joint Conference on Neural Networks*, 2020. ISBN 9781728169262. doi: 10.1109/IJCNN48605.2020.9206728. URL https://ieeexplore.ieee.org/document/9206728/.

Christian F. Baumgartner, Lisa M. Koch, Kerem Can Tezcan, Jia Xi Ang, and Ender Konukoglu. Visual Feature Attribution Using Wasserstein GANs. In *Computer Vision and Pattern Recognition*, 2018. ISBN 9781538664209. doi: 10.1109/CVPR.2018.00867. URL http://arxiv.org/abs/1711.08998.

Sara Beery, Grant Van Horn, and Pietro Perona. Recognition in Terra Incognita. In *European Conference on Computer Vision*, 2018. ISBN 9783030012694. doi: 10.1007/978-3-030-01270-0{_}28. URL http://arxiv.org/abs/1807.04975.

Pierre Chambon, Christian Bluethgen, Jean-Benoit Delbrouck, Rogier der Sluijs, Małgorzata Połacin, Juan Manuel Zambrano Chaves, Tanishq Mathew Abraham, Shivanshu Purohit, Curtis P Langlotz, and Akshay Chaudhari. RoentGen: Vision-Language Foundation Model for Chest X-ray Generation, 2022. URL https://arxiv.org/abs/2211.12737.

Joseph Paul Cohen, Rupert Brooks, Sovann En, Evan Zucker, Anuj Pareek, Matthew P. Lungren, and Akshay Chaudhari. Gifsplanation via Latent Shift: A Simple Autoencoder Approach to Counterfactual Generation for Chest X-rays. *Medical Imaging with Deep Learning*, 2021. URL https://openreview.net/forum?id=rnunjvgxAMt.

Paul R. Ehrlich, David S. Dobkin, and Darryl Wheye. *The Birder's Handbook*. Simon & Schuster, New York, NY, first edition, 1988. ISBN 978-0-671-65989-9.

Patrick Esser, Robin Rombach, and Björn Ommer. Taming transformers for high-resolution image synthesis. In *Computer Vision and Pattern Recognition*, 2021. ISBN 9781665445092. doi: 10.1109/CVPR46437.2021.01268. URL http://arxiv.org/abs/2012.09841.

Robert Geirhos, Jörn-Henrik Jacobsen, Claudio Michaelis, Richard Zemel, Wieland Brendel, Matthias Bethge, and Felix A. Wichmann. Shortcut learning in deep neural networks. *Nature Machine Intelligence*, 11 2020. ISSN 2522-5839. doi: 10.1038/s42256-020-00257-z. URL http://www.nature.com/articles/s42256-020-00257-z.

Kyle A. Hasenstab, Justin Huynh, Samira Masoudi, Guilherme M. Cunha, Michael Pazzani, and Albert Hsiao. Feature Interpretation Using Generative Adversarial Networks (FIGAN): A Framework for Visualizing a CNN's Learned Features. *IEEE Access*, 2023. ISSN 2169-3536. doi: 10.1109/ACCESS.2023.3236575. URL https://ieeexplore.ieee.org/document/10015730/.

Shalmali Joshi, Oluwasanmi Koyejo, Been Kim, and Joydeep Ghosh. xGEMs: Generating Examplars to Explain Black-Box Models, 2018. URL http://arxiv.org/abs/1806.08867.

Tero Karras, Timo Aila, Samuli Laine, and Jaakko Lehtinen. Progressive Growing of GANs for Improved Quality, Stability, and Variation. In *International Conference on Learning Representations*, 2018. URL https://arxiv.org/abs/1710.10196v3.

Tero Karras, Samuli Laine, and Timo Aila. A Style-Based Generator Architecture for Generative Adversarial Networks. In *Transactions on Pattern Analysis and Machine Intelligence*, 12 2021. URL https://arxiv.org/abs/1812.04948.

Been Kim, Martin Wattenberg, Justin Gilmer, Carrie Cai, James Wexler, Fernanda Viegas, and Rory Sayres. Interpretability beyond feature attribution: Quantitative Testing with Concept Activation Vectors (TCAV). In *International Conference on Machine Learning*, 2018. ISBN 9781510867963. URL http://arxiv.org/abs/1711.11279.

Narine Kokhlikyan, Vivek Miglani, Miguel Martin, Edward Wang, Bilal Alsallakh, Jonathan Reynolds, Alexander Melnikov, Natalia Kliushkina, Carlos Araya, Siqi Yan, and Orion Reblitz-Richardson. Captum: A unified and generic model interpretability library for PyTorch, 2020.

Ivan Krasin, Tom Duerig, Neil Alldrin, Vittorio Ferrari, Sami Abu-El-Haija, Alina Kuznetsova, Hassan Rom, Jasper Uijlings, Stefan Popov, Shahab Kamali, Matteo Malloci, Jordi Pont-Tuset, Andreas Veit, Serge Belongie, Victor Gomes, Abhinav Gupta, Chen Sun, Gal Chechik, David Cai, Zheyun Feng, Dhyanesh Narayanan, and Kevin Murphy. Openimages: A public dataset for large-scale multi-label and multi-class image classification. *Dataset available from https://storage.googleapis.com/openimages/web/index.html*, 2017.

David Krueger, Ethan Caballero, Joern Henrik Jacobsen, Amy Zhang, Jonathan Binas, Dinghuai Zhang, Remi Le Priol, and Aaron Courville. Out-of-Distribution Generalization via Risk Extrapolation. In *International Conference of Machine Learning*, 2021. ISBN 9781713845065. URL http://arxiv.org/abs/2003.00688.

Evan Zheran Liu, Behzad Haghgoo, Annie S. Chen, Aditi Raghunathan, Pang Wei Koh, Shiori Sagawa, Percy Liang, and Chelsea Finn. Just Train Twice: Improving Group Robustness without Training Group Information. In *International Conference on Machine Learning*, 7 2021. URL http://arxiv.org/abs/2107.09044.

Ziwei Liu, Ping Luo, Xiaogang Wang, and Xiaoou Tang. Deep learning face attributes in the wild. In *International Conference on Computer Vision*, 2015. ISBN 9781467383912. doi: 10.1109/ICCV.2015.425. URL https://arxiv.org/abs/1411.7766.

Mehdi Mirza and Simon Osindero. Conditional Generative Adversarial Nets, 2014. URL http://arxiv.org/abs/1411.1784.

Jose G. Moreno-Torres, Troy Raeder, Rocío Alaiz-Rodríguez, Nitesh V. Chawla, and Francisco Herrera. A unifying view on dataset shift in classification. *Pattern Recognition*, 1 2012. ISSN 0031-3203. doi: 10.1016/J.PATCOG.2011.06.019.

Chris Olah, Alexander Mordvintsev, and Ludwig Schubert. Feature Visualization. *Distill*, 2017. ISSN 2476-0757. doi: 10.23915/distill.00007. URL https://distill.pub/2017/feature-visualization.

Chris Olah, Nick Cammarata, Ludwig Schubert, Gabriel Goh, Michael Petrov, and Shan Carter. Zoom In: An Introduction to Circuits. *Distill*, 2020. ISSN 2476-0757. doi: 10.23915/distill.00024.001. URL https://distill.pub/2020/circuits/zoom-in.

Adam Paszke, Sam Gross, Francisco Massa, Adam Lerer, James Bradbury, Gregory Chanan, Trevor Killeen, Zeming Lin, Natalia Gimelshein, Luca Antiga, Alban Desmaison, Andreas Köpf, Edward Yang, Zach DeVito, Martin Raison, Alykhan Tejani, Sasank Chilamkurthy, Benoit Steiner, Lu Fang, Junjie Bai, and Soumith Chintala. PyTorch: An Imperative Style, High-Performance Deep Learning Library. *Neural Information Processing Systems*, 12 2019. URL https://arxiv.org/abs/1912.01703.

Judea Pearl. *Causality*. Cambridge University Press, 9 2009. ISBN 9780511803161. doi: 10.1017/CBO9780511803161. URL https://www.cambridge.org/core/product/identifier/9780511803161/type/book.

Marco Tulio Ribeiro, Sameer Singh, and Carlos Guestrin. "Why Should I Trust You?": Explaining the Predictions of Any Classifier. In *Knowledge Discovery and Data Mining*, 2016. doi: 10.1145/2939672.2939778. URL https://arxiv.org/abs/1602.04938.

Laura Rieger, Chandan Singh, W. James Murdoch, and Bin Yu. Interpretations are useful: Penalizing explanations to align neural networks with prior knowledge. In *International Conference on Machine Learning*, 9 2020. ISBN 9781713821120. URL http://arxiv.org/abs/1909.13584.

Andrew Ross, Michael C Hughes, and Finale Doshi-Velez. Right for the Right Reasons: Training Differentiable Models by Constraining their Explanations. In *International Joint Conference on Artificial Intelligence*, 2017. URL https://github.com/dtak/rrr.

Shiori Sagawa, Pang Wei Koh, Tatsunori B. Hashimoto, and Percy Liang. Distributionally Robust Neural Networks for Group Shifts: On the Importance of Regularization for Worst-Case Generalization. *International Conference on Learning Representations*, 11 2020. URL http://arxiv.org/abs/1911.08731.

Pouya Samangouei, Ardavan Saeedi, Liam Nakagawa, and Nathan Silberman. ExplainGAN: Model Explanation via Decision Boundary Crossing Transformations. In *European Conference on Computer Vision*, 2018. URL https://openaccess.thecvf.com/content_ECCV_2018/html/Nathan_Silberman_ExplainGAN_Model_Explanation_ECCV_2018_paper.html.

Ioannis Sarridis, Christos Koutlis, Symeon Papadopoulos, and Christos Diou. FLAC: Fairness-Aware Representation Learning by Suppressing Attribute-Class Associations. *arXiv:2304.14252*, 4 2023. URL http://arxiv.org/abs/2304.14252.

Kathryn Schutte, Olivier Moindrot, Paul Hérent, Jean-Baptiste Schiratti, and Simon Jégou. Using StyleGAN for Visual Interpretability of Deep Learning Models on Medical Images. In *Medical Imaging meets NeurIPS*, 2020. URL https://arxiv.org/abs/2101.07563.

Jarrel C.Y. Seah, Jennifer S.N. Tang, Andy Kitchen, Frank Gaillard, and Andrew F. Dixon. Chest radiographs in congestive heart failure: Visualizing neural network learning. *Radiology*, 2019. ISSN 15271315. doi: 10.1148/radiol.2018180887.

Karen Simonyan, Andrea Vedaldi, and Andrew Zisserman. Deep Inside Convolutional Networks: Visualising Image Classification Models and Saliency Maps. In *International Conference on Learning Representations*, 2014. URL http://arxiv.org/abs/1312.6034.

Chandan Singh, Guha Balakrishnan, and Pietro Perona. Matched sample selection with GANs for mitigating attribute confounding. *arXiv:2103.13455*, 2021. URL http://arxiv.org/abs/2103.13455.

Sumedha Singla, Motahhare Eslami, Brian Pollack, Stephen Wallace, and Kayhan Batmanghelich. Explaining the black-box smoothly—A counterfactual approach. *Medical Image Analysis*, 2023. ISSN 13618423. doi: 10.1016/j.media.2022.102721. URL https://arxiv.org/abs/2101.04230.

Jost Tobias Springenberg, Alexey Dosovitskiy, Thomas Brox, and Martin Riedmiller. Striving for Simplicity: The All Convolutional Net. In *International Conference on Learning Representations Workshop*, 2015. URL http://arxiv.org/abs/1412.6806.

Mukund Sundararajan, Ankur Taly, and Qiqi Yan. Axiomatic Attribution for Deep Networks. In *International Conference on Machine Learning*, 2017. URL http://arxiv.org/abs/1703.01365.

Simon Vandenhende, Stamatios Georgoulis, Bert De Brabandere, and Luc Van Gool. Branched Multi-Task Networks: Deciding What Layers To Share. *British Machine Vision Conference*, 4 2020. URL http://arxiv.org/abs/1904.02920.

Sahil Verma, Varich Boonsanong, Minh Hoang, Keegan E. Hines, John P. Dickerson, and Chirag Shah. Counterfactual Explanations and Algorithmic Recourses for Machine Learning: A Review. In *Neural Information Processing Systems (NeurIPS) Retrospectives Workshop*, 10 2020. doi: 10.48550/arxiv.2010.10596. URL http://arxiv.org/abs/2010.10596.

Catherine Wah, Steve Branson, Peter Welinder, Pietro Perona, and Serge Belongie. The Caltech-UCSD Birds-200-2011 Dataset, 2011.

Mitchell Wortsman, Gabriel Ilharco, Samir Yitzhak Gadre, Rebecca Roelofs, Raphael Gontijo-Lopes, Ari S. Morcos, Hongseok Namkoong, Ali Farhadi, Yair Carmon, Simon Kornblith, and Ludwig Schmidt. Model soups: averaging weights of multiple fine-tuned models improves accuracy without increasing inference time. In *International Conference on Machine Learning*, 3 2022. URL http://arxiv.org/abs/2203.05482.

Huimin Zeng, Zhenrui Yue, Ziyi Kou, Yang Zhang, Lanyu Shang, and Dong Wang. Fairness-aware training of face attribute classifiers via adversarial robustness. *Knowledge-Based Systems*, 2023. ISSN 09507051. doi: 10.1016/j.knosys.2023.110356. URL https://doi.org/10.1016/j.knosys.2023.110356.

A Appendix

	blurry	gray_hair	bald	wearing_hat	male	sideburns	wearing_necktie	mustache	chubby	big_nose	double_chin	receding_hairline	goatee	narrow_eyes	bags_under_eyes	eyeglasses	big_lips	black_hair	no_beard	smiling	mouth_slightly_open	high_cheekbones	wearing_earrings	wearing_necklace	wavy_hair	pointy_nose	blond_hair	bangs	heavy_makeup	wearing_lipstick	rosy_cheeks	arched_eyebrows	oval_face	attractive	pale_skin	young	straight_hair	bushy_eyebrows	5_o_clock_shadow	brown_hair
blurry	1.00	0.01	0.00	-0.16	0.15	-0.12	-0.01	0.04	-0.02	-0.18	0.02	0.01	-0.10	0.05	-0.13	-0.04	-0.08	-0.02	0.08	-0.09	-0.03	-0.05	-0.01	-0.06	-0.03	-0.07	0.04	-0.03	-0.07	-0.25	-0.02	-0.12	-0.01	-0.19	-0.10	0.00	-0.00	-0.07	0.02	-0.05
gray_hair	-0.00	1.00	-0.05	-0.03	0.04	-0.02	0.11	0.07	-0.05	0.14	0.03	0.31	-0.00	-0.04	0.15	0.01	-0.07	-0.01	0.06	-0.04	-0.04	-0.05	-0.03	0.00	0.02	0.03	-0.22	-0.06	-0.07	-0.05	-0.00	-0.11	-0.11	-0.09	-0.00	-0.24	-0.04	-0.07	-0.18	-0.03
bald	-0.00	-0.12	1.00	-0.05	0.02	0.04	0.04	-0.01	0.12	0.07	0.09	-0.23	0.21	0.00	0.06	-0.02	-0.00	-0.05	-0.10	-0.00	-0.07	-0.01	0.01	-0.01	-0.01	0.02	-0.02	-0.01	-0.01	-0.01	-0.00	0.05	0.05	-0.02	-0.00	-0.05	-0.10	0.04	0.01	-0.02
wearing_hat	0.00	-0.01	-0.06	1.00	0.09	0.04	0.01	-0.02	0.07	0.12	0.08	-0.04	0.00	-0.07	0.19	0.00	-0.13	-0.39	-0.00	-0.03	-0.03	-0.07	-0.10	-0.04	-0.05	-0.01	-0.01	-0.03	-0.09	-0.11	-0.01	-0.19	-0.08	-0.10	-0.02	-0.22	-0.16	-0.05	0.06	-0.00
male	-0.00	0.05	0.08	0.02	1.00	0.07	0.10	0.06	0.04	0.19	0.09	-0.01	0.26	0.04	0.23	-0.01	-0.07	-0.04	-0.55	-0.05	-0.07	-0.11	-0.31	-0.12	-0.03	-0.05	-0.06	-0.05	-0.51	-0.69	-0.05	-0.21	-0.15	-0.16	-0.04	-0.10	0.05	0.09	0.36	0.03
sideburns	-0.00	0.00	-0.01	0.00	0.02	1.00	0.01	0.01	0.12	0.01	-0.06	-0.06	0.11	0.01	0.06	-0.00	-0.09	-0.03	-0.18	-0.03	-0.11	-0.09	-0.07	-0.01	0.00	-0.03	-0.01	-0.00	-0.02	-0.02	0.00	-0.08	-0.02	0.01	-0.01	-0.08	0.01	-0.05	-0.04	0.04
wearing_necktie	-0.00	0.04	0.04	-0.00	0.01	0.02	1.00	0.03	0.12	0.10	0.14	0.05	0.03	0.03	0.13	0.01	-0.02	-0.03	-0.00	-0.00	-0.03	-0.03	-0.02	-0.02	-0.03	0.01	-0.01	-0.00	-0.01	-0.01	0.01	-0.06	-0.06	-0.01	-0.01	-0.10	0.06	0.04	0.00	-0.01
mustache	0.00	0.01	-0.05	-0.01	0.01	-0.17	0.07	1.00	0.04	0.18	0.10	0.12	0.31	0.12	0.09	-0.00	0.14	0.12	-0.20	-0.09	-0.32	-0.00	0.05	0.05	-0.02	-0.04	-0.01	-0.00	-0.02	-0.02	0.01	0.05	-0.03	-0.03	-0.00	-0.12	0.01	0.13	-0.14	-0.05
chubby	0.00	0.02	0.06	0.01	0.01	0.11	0.11	0.05	1.00	0.28	0.64	0.04	0.01	0.08	0.10	0.00	0.06	0.04	-0.09	-0.02	-0.02	0.04	0.00	0.01	0.03	-0.23	-0.01	-0.00	0.01	-0.01	0.01	-0.13	-0.00	-0.22	-0.00	-0.30	-0.10	-0.08	0.02	-0.03
big_nose	-0.01	0.06	0.06	0.03	0.06	-0.05	0.05	0.13	0.27	1.00	0.30	0.13	0.14	0.05	0.53	0.01	0.19	0.04	-0.03	0.08	0.05	0.18	0.12	0.09	0.03	-0.36	-0.04	-0.03	-0.08	-0.06	0.01	0.05	-0.20	-0.42	-0.01	-0.37	-0.10	0.08	-0.02	-0.09
double_chin	-0.00	0.09	0.09	0.00	0.06	-0.09	0.10	0.05	0.69	0.40	1.00	0.10	-0.07	0.08	0.25	0.02	0.04	-0.01	0.21	0.19	0.09	0.21	-0.02	0.01	0.03	-0.17	-0.02	-0.01	-0.05	-0.05	0.04	-0.13	-0.09	-0.29	0.00	-0.37	-0.15	-0.08	-0.15	-0.03
receding_hairline	-0.00	0.15	-0.04	-0.01	-0.04	-0.14	0.02	0.03	0.08	0.18	0.11	1.00	-0.02	0.02	0.08	-0.01	0.04	0.08	0.21	-0.01	0.03	0.04	0.06	0.02	0.01	0.00	-0.02	-0.00	-0.02	0.01	-0.04	0.07	-0.14	-0.25	-0.00	-0.22	-0.17	-0.15	-0.26	-0.07
goatee	-0.00	-0.02	0.07	-0.00	0.02	-0.11	0.01	0.20	0.02	0.12	0.02	0.03	1.00	0.01	0.00	-0.00	0.08	0.00	-0.15	0.08	0.08	0.06	-0.00	0.01	-0.03	-0.10	-0.01	0.02	-0.00	-0.00	0.00	-0.02	0.07	-0.00	-0.00	-0.03	0.01	-0.06	-0.35	-0.02
narrow_eyes	-0.00	-0.01	-0.00	-0.01	0.01	0.01	0.01	0.01	0.04	0.07	0.04	0.04	0.01	1.00	0.11	-0.05	0.08	0.00	0.00	0.06	0.08	0.05	0.02	0.01	-0.01	-0.06	-0.01	0.00	-0.12	-0.08	-0.03	-0.08	-0.15	-0.08	-0.01	0.04	0.05	0.06	0.00	0.02
bags_under_eyes	-0.00	0.06	0.05	0.02	0.02	0.03	0.06	0.01	0.08	0.51	0.11	0.07	0.00	-0.01	1.00	-0.07	-0.00	-0.07	0.03	0.06	0.02	0.18	0.00	0.04	-0.08	0.02	-0.04	-0.01	-0.13	-0.04	-0.05	-0.02	-0.32	-0.34	-0.01	-0.39	0.02	0.04	-0.03	0.02
eyeglasses	-0.00	0.02	0.01	0.00	-0.00	-0.02	0.02	0.00	0.03	0.10	0.04	0.02	0.04	-0.05	-0.01	1.00	-0.04	-0.02	0.03	0.02	0.06	0.02	-0.01	-0.00	-0.01	-0.01	0.00	-0.02	-0.03	-0.02	-0.00	-0.05	-0.00	-0.07	-0.01	-0.12	0.01	-0.01	-0.05	0.00
big_lips	-0.00	-0.02	-0.01	0.02	-0.02	-0.11	-0.01	0.02	0.06	0.31	0.05	0.04	0.02	0.03	0.00	-0.00	1.00	0.22	-0.01	0.06	0.25	0.09	0.26	0.17	0.09	-0.12	-0.07	0.01	0.31	0.17	-0.03	0.27	-0.18	-0.00	0.04	0.25	-0.09	0.12	0.00	-0.06
black_hair	-0.00	-0.00	-0.03	-0.01	-0.00	-0.02	-0.00	0.02	0.03	0.09	-0.00	0.02	0.01	0.00	-0.03	-0.00	0.12	1.00	0.02	0.02	-0.04	0.05	-0.03	0.00	-0.04	-0.08	-0.00	-0.01	0.02	0.02	-0.05	0.09	-0.05	-0.01	-0.02	0.11	0.06	0.11	-0.01	-0.19
no_beard	0.01	0.03	-0.01	-0.00	-0.06	-0.26	0.04	-0.04	0.04	0.01	0.08	0.00	-0.19	-0.00	0.01	-0.00	-0.02	0.02	1.00	0.11	0.06	0.13	0.02	-0.01	-0.01	-0.00	0.01	0.00	0.02	0.06	0.00	0.06	0.02	-0.01	0.00	-0.04	0.04	0.03	-0.61	-0.02
smiling	-0.00	0.01	0.01	-0.00	-0.01	-0.03	0.01	0.01	-0.03	0.11	0.06	-0.03	0.03	0.02	0.14	0.01	0.04	-0.01	0.01	1.00	0.26	0.63	-0.01	0.04	-0.00	0.08	0.02	0.01	0.09	0.04	0.19	0.07	0.12	0.15	-0.00	-0.02	-0.01	-0.04	-0.01	-0.04
mouth_slightly_open	0.00	0.00	-0.00	0.00	-0.00	-0.02	-0.01	-0.03	-0.03	-0.01	-0.01	-0.01	-0.03	0.05	0.06	-0.01	0.02	-0.01	0.08	0.39	1.00	0.29	-0.04	-0.02	-0.03	0.03	0.01	0.00	-0.01	0.00	0.05	-0.02	-0.04	-0.03	-0.02	-0.01	0.02	-0.16	-0.06	-0.02
high_cheekbones	-0.00	0.00	0.00	-0.01	-0.08	-0.02	-0.01	-0.01	0.00	0.16	0.04	0.01	-0.01	0.02	0.21	-0.00	0.00	0.02	0.10	0.63	0.17	1.00	0.15	0.04	0.05	0.07	0.01	0.01	0.10	0.10	0.26	0.19	0.05	0.00	-0.06	-0.10	-0.05	-0.06	-0.08	-0.03
wearing_earrings	-0.00	0.00	-0.00	-0.01	-0.11	0.00	-0.02	0.00	0.01	0.06	0.01	0.06	-0.00	0.02	-0.03	-0.01	0.10	0.01	0.01	0.05	0.06	0.13	1.00	0.07	0.00	0.06	-0.00	0.00	0.20	0.14	0.13	0.18	-0.06	-0.01	-0.01	-0.02	-0.06	-0.05	-0.01	-0.02
wearing_necklace	-0.00	0.01	0.00	-0.00	-0.01	-0.00	-0.01	-0.00	0.02	0.35	0.13	0.02	-0.00	0.01	0.29	-0.00	0.18	-0.00	0.00	0.05	0.04	0.09	0.12	1.00	0.05	0.07	0.00	0.00	0.05	0.07	0.12	0.24	-0.47	-0.39	-0.06	-0.23	-0.07	-0.11	-0.00	-0.07
wavy_hair	0.00	0.00	-0.01	-0.01	-0.00	0.00	-0.00	-0.00	0.01	0.01	0.01	-0.02	-0.00	0.01	-0.03	0.00	0.04	-0.03	-0.00	0.03	0.02	0.05	0.01	-0.01	1.00	-0.00	-0.00	0.00	0.11	0.04	0.05	0.07	0.03	0.06	0.00	-0.03	-0.71	-0.02	0.00	0.11
pointy_nose	0.00	0.01	0.00	-0.01	-0.09	-0.02	0.00	-0.01	-0.22	-0.47	-0.10	-0.05	-0.06	-0.04	-0.13	-0.00	-0.09	-0.07	0.05	0.24	0.13	0.25	0.12	0.02	-0.03	1.00	0.07	-0.00	0.28	0.17	0.36	0.27	0.05	0.34	-0.03	-0.04	-0.01	0.09	0.02	0.00
blond_hair	0.00	-0.03	-0.01	-0.01	-0.10	-0.01	-0.01	-0.00	-0.03	-0.28	-0.07	-0.11	-0.02	-0.04	-0.18	-0.02	-0.07	-0.01	0.02	0.05	-0.03	0.06	0.01	0.05	0.04	0.15	1.00	0.05	0.31	0.21	0.09	0.10	0.25	0.35	0.01	0.20	0.03	-0.13	-0.01	-0.20
bangs	-0.00	-0.01	-0.00	-0.07	-0.09	-0.02	-0.00	-0.00	-0.03	-0.05	-0.04	-0.00	0.00	0.00	-0.02	-0.00	0.05	0.03	0.03	0.11	0.00	0.15	0.13	0.05	-0.06	0.04	0.07	1.00	0.21	0.17	0.09	-0.01	0.17	0.23	-0.00	0.06	0.04	-0.02	-0.06	-0.02
heavy_makeup	0.00	-0.00	-0.00	-0.00	-0.07	0.00	-0.00	-0.00	-0.01	-0.20	-0.04	-0.03	-0.00	-0.04	-0.32	-0.00	0.13	0.01	0.00	0.08	0.17	0.11	0.26	0.01	0.11	0.10	0.03	0.02	1.00	0.36	0.24	0.31	0.34	0.45	0.03	0.15	-0.09	0.06	-0.01	-0.04
wearing_lipstick	0.00	-0.02	-0.01	-0.01	-0.47	-0.00	-0.01	-0.00	-0.02	-0.25	-0.05	-0.06	-0.00	-0.05	-0.36	-0.03	0.19	0.01	0.02	0.12	0.19	0.21	0.32	0.15	0.11	0.20	0.05	0.03	1.10	1.00	0.17	0.53	0.32	0.58	0.00	0.09	-0.05	0.01	-0.05	-0.02
rosy_cheeks	0.00	-0.00	-0.01	0.00	-0.01	0.00	-0.00	-0.00	0.01	-0.04	0.02	-0.03	-0.00	-0.02	-0.12	-0.01	0.02	-0.02	0.00	0.14	0.04	0.15	0.08	0.05	0.04	0.36	0.01	0.01	0.22	0.04	1.00	0.22	0.15	0.18	-0.03	0.02	-0.04	0.02	-0.00	-0.05
arched_eyebrows	0.00	-0.00	0.01	-0.00	-0.03	-0.00	0.00	0.00	-0.00	0.05	-0.00	0.03	0.00	-0.06	-0.00	-0.00	0.10	-0.00	-0.00	-0.01	-0.03	0.06	0.08	0.07	0.02	0.14	0.01	-0.01	0.23	0.15	0.07	1.00	-0.06	0.07	-0.00	0.01	-0.05	-0.01	0.00	-0.03
oval_face	0.01	-0.01	-0.01	-0.00	-0.08	0.00	-0.01	-0.00	-0.04	-0.28	-0.09	-0.12	0.00	-0.16	-0.35	-0.00	-0.04	0.01	0.01	0.10	-0.07	0.03	-0.05	-0.15	0.05	0.02	0.06	0.03	0.47	0.15	0.18	0.14	1.00	0.64	0.02	0.35	0.04	0.15	-0.01	0.02
attractive	0.00	-0.02	-0.01	-0.00	-0.06	0.00	-0.00	-0.00	-0.13	-0.39	-0.12	-0.15	0.00	-0.03	-0.37	-0.02	0.01	-0.01	-0.01	0.10	-0.01	-0.00	-0.04	-0.18	0.05	0.19	0.05	0.03	0.60	0.22	0.10	0.25	0.58	1.00	0.05	0.40	0.07	0.17	0.04	0.05
pale_skin	-0.00	-0.00	-0.00	-0.02	-0.08	-0.01	0.00	0.00	-0.02	-0.10	-0.01	-0.04	0.00	-0.01	-0.11	-0.00	0.09	-0.01	0.02	-0.02	0.02	-0.14	-0.11	-0.03	0.03	-0.02	0.01	0.03	0.21	0.12	-0.05	0.02	0.09	0.24	1.00	0.07	0.01	0.00	-0.00	-0.05
young	-0.00	-0.02	-0.01	0.00	-0.01	-0.01	-0.00	-0.01	-0.10	-0.32	-0.14	-0.09	-0.04	0.01	-0.42	-0.00	0.19	0.06	0.06	-0.03	-0.03	-0.11	-0.12	-0.16	-0.10	-0.06	0.04	-0.02	0.44	0.09	0.00	0.10	0.38	0.78	0.03	1.00	0.20	0.14	-0.01	0.03
straight_hair	0.00	-0.01	-0.01	-0.04	0.05	-0.01	0.01	-0.00	-0.02	-0.07	-0.05	-0.05	-0.02	0.02	-0.04	-0.00	0.01	0.07	0.06	0.01	0.00	-0.03	-0.10	-0.02	-0.48	-0.02	0.03	0.03	0.01	-0.04	-0.01	-0.09	0.04	0.12	0.00	0.12	1.00	0.05	-0.03	-0.00
bushy_eyebrows	0.00	-0.01	-0.00	-0.00	0.02	-0.01	0.01	0.01	-0.01	0.07	0.00	-0.03	-0.02	0.02	0.02	-0.00	0.06	0.09	0.02	0.00	-0.03	-0.02	-0.02	-0.00	-0.01	0.05	-0.01	-0.01	0.02	-0.02	-0.00	0.07	0.03	0.10	-0.00	0.06	0.04	1.00	0.02	-0.06
5_o_clock_shadow	-0.00	-0.02	-0.03	0.00	0.05	0.12	0.03	-0.04	-0.02	-0.07	0.00	-0.10	-0.37	0.01	-0.03	-0.00	0.05	0.03	-0.36	-0.01	-0.01	-0.06	-0.02	-0.01	0.00	0.08	-0.01	0.00	-0.02	-0.03	0.00	0.04	-0.00	0.17	-0.01	0.25	0.04	0.08	1.00	0.01
brown_hair	0.00	-0.02	-0.01	-0.00	0.01	0.02	-0.02	-0.01	-0.04	-0.16	-0.06	-0.06	0.01	0.02	0.02	-0.00	-0.06	-0.27	-0.05	-0.02	-0.02	-0.03	-0.07	-0.10	0.18	0.01	-0.21	-0.00	-0.06	-0.04	-0.07	-0.09	0.01	0.11	-0.02	0.07	-0.08	-0.09	0.05	1.00

Figure 7: The complete matrix of relative changes for all classifiers. Ordering is determined by clustering to group similar classifiers.

A.1 Rectifying bias by composing classifiers

This section demonstrates the use of CF alignment to fix model bias in classifiers. We can reuse the relative change between model predictions as a loss function that can be minimized.

This section just serves as an example to better understand a use of the CF alignment idea. We don't claim this method is competitive to other methods which correct model bias and spurious correlations. Related approaches include averaging model weights Wortsman et al. (2022) or methods of invariant optimization Sagawa et al. (2020); Krueger et al. (2021); Rieger et al. (2020); Zeng et al. (2023) and approaches for balanced dataset sampling Singh et al. (2021). Composing classifiers can change their response to specific samples that contain relevant features as shown in §4.4. By using this additive composition approach we avoid the variance of model training which makes it easy and reproducible to perform experiments.

First, we demonstrate a single example of correcting bias. In Fig. 8, the CF image and CF alignment plot for the *heavy_makeup* base classifier show unexpected reductions in lip size. Composing the model with the *big_lips* classifier using a negative coefficient causes the classifier to lower any feature change focused on the lips as this would increase the prediction of the composed classifier (where the goal of the CF is to decrease it). We can also visually observe other features that change, such as skin color, bushy eyebrows, and the amount that the mouth is open.

Next, this unbiasing is scaled up to a larger number of samples and classifiers. A collection of 12 classifiers that contain varying spurious relationships to a *big_nose* base classifier (shown in Fig. 9a) are modified to remove their bias until their relative change is as close to 0 as possible. This experiment is performed with

(a) As makeup is removed from the face, the lip size also shrinks.

(b) The lip size remains the same as the makeup is removed.

Figure 8: An example of a *big_lips* spurious correlation being corrected for the *heavy_makeup* classifier.

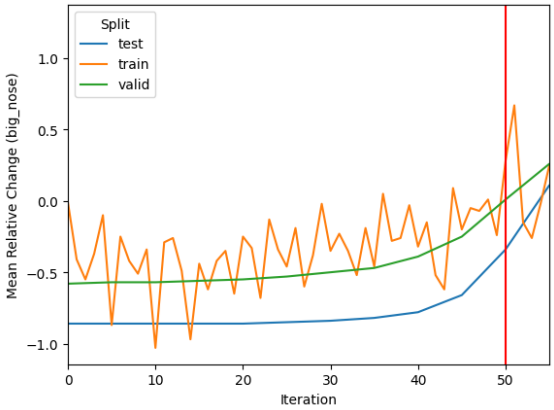

Figure 9: Training curves showing mean relative change during the optimization of a classifier with respect to the *big_nose* classifier during each iteration. The red vertical line is the early stopping point based on the validation set. This demonstrates how bias can be quantified and corrected using CF alignment.

A) Baseline

	mouth_slightly_open	big_nose	male	bushy_eyebrows	arched_eyebrows	smiling	high_cheekbones	pointy_nose	wearing_lipstick	heavy_makeup	oval_face	attractive	young
mouth_slightly_open	1.00	-0.20	-0.00	-0.04	-0.16	0.52	0.21	0.04	0.03	0.03	0.24	0.04	-0.07
big_nose	0.08	1.00	0.00	0.82	-0.01	0.61	0.55	-0.42	-0.06	-0.34	-0.36	-0.56	-0.02
male	-0.01	0.24	1.00	0.11	-0.02	-0.02	-0.09	-0.09	-0.39	-0.20	-0.03	-0.20	-0.01
bushy_eyebrows	0.07	-0.05	0.00	1.00	0.18	-0.01	-0.06	0.06	0.00	0.00	-0.03	0.12	0.19
arched_eyebrows	-0.01	0.25	0.00	0.02	1.00	-0.00	0.00	0.24	0.00	0.02	-0.33	-0.06	-0.01
smiling	0.33	0.25	-0.00	-0.00	0.05	1.00	0.90	0.02	0.00	0.01	0.12	0.13	-0.27
high_cheekbones	0.02	0.05	-0.01	-0.10	0.38	0.04	1.00	0.20	0.03	0.11	-0.06	-0.01	-0.16
pointy_nose	-0.05	-0.86	-0.00	0.08	-0.01	0.29	0.28	1.00	0.00	0.03	0.10	0.49	-0.00
wearing_lipstick	-0.05	-0.06	-0.41	-0.02	0.41	-0.01	0.02	0.14	1.00	1.26	0.06	0.52	-0.03
heavy_makeup	0.27	-0.03	-0.01	0.05	0.14	0.03	0.24	0.11	0.39	1.00	0.31	0.12	0.00
oval_face	0.11	-0.41	-0.00	0.16	-0.20	0.36	0.22	0.24	0.00	0.01	1.00	0.56	0.01
attractive	-0.04	-0.49	-0.08	0.20	0.08	0.09	-0.09	0.22	0.29	1.04	0.67	1.00	0.24
young	-0.02	-0.18	0.38	0.01	-0.02	-0.02	-0.19	-0.03	-0.25	-0.05	0.05	0.56	1.00

B) Optimized

	mouth_slightly_open	big_nose	male	bushy_eyebrows	arched_eyebrows	smiling	high_cheekbones	pointy_nose	wearing_lipstick	heavy_makeup	oval_face	attractive	young
mouth_slightly_open	1.00	-0.01	0.00	-0.02	-0.13	0.56	0.23	0.02	0.01	-0.01	-0.02	-0.03	-0.09
big_nose	0.08	1.00	0.00	0.82	-0.01	0.61	0.55	-0.42	-0.06	-0.34	-0.36	-0.56	-0.02
male	-0.01	-0.00	1.00	0.09	-0.04	-0.02	-0.10	-0.05	-0.34	-0.16	0.00	-0.12	-0.00
bushy_eyebrows	0.07	-0.05	0.00	1.00	0.18	-0.01	-0.06	0.06	0.00	0.00	-0.03	0.12	0.19
arched_eyebrows	-0.01	0.00	-0.00	0.01	1.00	-0.01	0.00	0.31	0.01	0.06	-0.16	0.08	-0.00
smiling	0.44	-0.01	-0.00	0.00	-0.08	1.00	0.79	0.02	0.01	0.02	0.19	0.35	-0.13
high_cheekbones	0.02	0.01	-0.02	-0.12	0.40	0.04	1.00	0.20	0.04	0.14	-0.03	-0.01	-0.16
pointy_nose	-0.07	0.11	0.00	0.09	0.01	0.38	0.69	0.94	-0.00	-0.01	-0.07	-0.13	-0.12
wearing_lipstick	-0.05	-0.00	-0.40	0.00	0.43	-0.01	0.03	0.11	1.00	1.26	0.06	0.48	-0.03
heavy_makeup	0.27	-0.03	-0.01	0.05	0.14	0.03	0.24	0.11	0.39	1.00	0.31	0.12	0.00
oval_face	-0.06	0.04	-0.00	0.17	-0.14	0.41	0.43	-0.22	0.00	0.01	0.99	0.45	0.01
attractive	-0.04	-0.49	-0.08	0.20	0.08	0.09	-0.09	0.22	0.29	1.04	0.67	1.00	0.24
young	-0.02	-0.02	0.75	0.01	-0.01	-0.02	-0.20	-0.07	-0.49	-0.13	0.04	0.54	1.00

Figure 10: CF alignment matrices before and after optimization to remove the bias for *big_nose* on a hold out test set. The figure shows a dramatic reduction in relative change for most classifiers and *big_nose* with limited residual impact on other relationships.

a train, validation, and hold out test set in order to demonstrate the generalization of this unbiasing process to unseen data.

The classifiers are modified using a single coefficient (β) such that the resulting classifier is

$$f'_{target}(x) = f_{target}(x) + \beta f_{big_nose}(x) \tag{5}$$

Optimization to compute each β is performed using a pseudo gradient descent where the gradient is approximated by the mean relative change between the target classifier and the *big_nose* classifier. By subtracting the relative change from β, scaled by a learning rate, the relative change (ψ) with that classifier will be reduced. All together our training objective (including momentum) is

$$\beta_n = 0.001\psi(f_{target}, f_{big_nose}) + 0.1\beta_{n-1} \tag{6}$$

We find that using small minibatches of 10 samples works well because the computation time for each CF can take over 1 second on a GPU. Additionally, training with samples which induce a small change in the base classifier during the CF generation process can be challenging. As the classifiers are modified, this base change is reduced, which causes the relative change to become more erratic and prevents the optimization from converging. To prevent this, we use samples with a base change > 0.6.

The resulting training metrics in Fig. 9 show model biases being minimized similar to a differentiable training loss. Looking at the mean relative change allows us to summarize the bias of the model with respect to the *big_nose* classifier who's relationship we aim to remove. We observe a bias generalization gap between the train, valid, and test sets, indicating some degree of overfitting. Early stopping (red vertical line) is used on the validation set to determine the optimal parameters. We use momentum during training to average over the noise.

The resulting reduction in bias is shown per classifier before and after training in Fig 10. 10 of the 12 classifiers being optimized have the bias considerably reduced (closer to 0) except for *attractive* and *big_nose*, which could be the result of overlapping features used by both classifiers that cannot be changed.

iter	mouth_slightly_open	big_nose	male	bushy_eyebrows	arched_eyebrows	smiling	high_cheekbones	pointy_nose	wearing_lipstick	heavy_makeup	oval_face	attractive	young	Coefficient
0	-0.01	-0.01	-0.00	-0.00	0.18	0.04	0.79	1.00	0.01	0.05	-0.06	0.00	-0.02	0.00
5	0.00	-0.87	-0.02	-0.00	0.10	0.32	0.45	1.00	0.03	0.04	0.23	0.35	-0.02	0.00
10	0.51	-1.03	-0.04	0.12	0.06	0.75	0.84	1.01	0.26	1.09	0.04	0.80	-0.07	0.01
15	-0.00	-0.44	-0.00	0.00	0.09	0.00	0.00	1.00	0.00	0.01	0.43	0.26	0.00	0.01
20	-0.01	-0.25	-0.01	0.37	0.52	0.00	0.00	1.00	0.01	0.03	0.25	0.23	-0.01	0.02
25	0.00	-0.46	-0.11	-0.00	0.11	0.01	0.05	1.02	0.42	0.18	0.03	0.12	0.02	0.03
30	0.25	-0.35	0.00	0.02	0.11	0.96	0.31	1.02	0.00	0.00	-0.02	0.15	0.19	0.05
35	0.01	-0.46	-0.01	0.03	0.03	0.68	0.24	1.04	0.06	0.25	0.03	0.50	-0.04	0.09
40	0.88	-0.32	-0.00	0.03	0.19	0.14	0.12	1.04	0.03	0.15	0.29	0.29	-0.02	0.13
45	0.16	-0.20	-0.00	0.52	0.06	0.03	0.18	1.04	0.00	0.01	-0.18	0.19	0.00	0.21
50	0.01	0.28	0.00	0.01	0.39	0.04	0.04	0.91	-0.00	-0.00	-0.12	-0.02	-0.04	0.32
55	-0.03	0.25	0.00	0.45	0.13	-0.01	-0.01	0.88	0.00	0.00	-0.18	-0.06	-0.36	0.50
60	0.37	-0.58	-0.01	0.00	0.13	0.93	1.02	1.29	0.10	0.97	-0.57	0.55	-0.12	0.50

iter	mouth_slightly_open	big_nose	male	bushy_eyebrows	arched_eyebrows	smiling	high_cheekbones	pointy_nose	wearing_lipstick	heavy_makeup	oval_face	attractive	young	Coefficient
0	0.31	0.11	0.00	-0.01	-0.12	1.00	0.64	0.04	-0.01	-0.20	-0.01	0.01	-0.31	0.00
5	0.02	-0.2	0.00	0.06	0.04	1.00	0.43	0.05	0.00	0.00	0.04	0.28	0.07	-0.00
10	0.26	0.19	-0.00	-0.08	-0.06	1.00	0.75	0.08	0.00	-0.01	0.04	0.08	-0.01	-0.00
15	0.07	0.19	0.00	-0.41	-0.04	1.00	0.81	-0.02	-0.01	-0.01	0.16	0.14	-0.04	-0.00
20	0.33	0.00	-0.00	-0.00	0.26	1.00	0.79	0.13	0.00	0.00	0.09	0.03	-0.08	-0.00
25	0.01	0.09	-0.00	0.04	0.11	1.00	0.15	0.03	0.00	0.00	0.04	0.22	0.02	-0.01
30	0.01	0.08	-0.00	-0.00	0.03	1.00	0.63	0.04	0.00	0.02	0.13	0.08	-0.00	-0.01
35	1.06	0.01	-0.00	0.05	0.07	1.00	0.66	0.01	0.00	0.00	0.01	0.01	0.01	-0.01
40	0.13	-0.19	-0.00	-0.05	0.03	1.00	0.15	0.37	0.01	0.05	0.20	0.50	-0.01	-0.02
45	-0.01	0.05	-0.00	0.00	0.07	1.00	0.91	0.04	0.04	0.27	0.21	0.23	0.00	-0.03
50	0.00	-0.03	-0.01	-0.00	0.00	1.00	0.55	0.09	0.07	0.06	0.03	0.13	-0.13	-0.05
55	1.29	0.00	-0.00	-0.00	0.20	1.00	0.53	-0.00	0.00	0.00	0.22	0.14	-0.00	-0.08

iter	mouth_slightly_open	big_nose	male	bushy_eyebrows	arched_eyebrows	smiling	high_cheekbones	pointy_nose	wearing_lipstick	heavy_makeup	oval_face	attractive	young	Coefficient
0	0.11	-0.48	-0.02	0.52	0.39	0.21	0.04	0.15	0.03	0.03	0.45	1.00	0.42	0.00
5	-0.04	-0.66	-0.01	0.15	0.28	0.04	0.02	0.19	0.03	0.30	0.17	1.00	0.25	0.00
10	-0.41	-0.29	-0.04	0.19	0.05	0.00	0.03	0.25	0.14	0.21	0.67	1.00	0.02	0.00
15	-0.05	-0.81	-0.01	0.04	0.03	-0.06	-0.26	0.53	0.02	0.11	0.93	1.01	0.22	0.01
20	-0.14	-0.47	-0.01	0.00	0.25	0.02	-0.03	0.23	0.27	0.89	-0.01	1.01	0.06	0.02
25	-0.00	0.41	-0.01	0.61	0.96	0.05	0.33	0.23	0.12	0.90	0.90	0.99	0.10	0.03
30	-0.02	-0.44	-0.02	0.16	0.06	0.02	0.01	0.09	0.46	0.84	1.00	1.02	0.23	0.05
35	-0.01	-0.42	-0.01	0.15	-0.00	0.15	0.07	0.40	0.23	1.02	0.46	1.03	0.11	0.07
40	-0.01	-0.31	-0.02	0.28	0.04	0.28	0.11	-0.13	0.05	0.17	0.72	1.04	0.64	0.12
45	0.01	-0.26	-0.37	0.46	0.04	0.58	0.12	0.11	0.87	0.82	0.62	1.04	0.32	0.17
50	-0.01	0.30	-0.01	0.13	0.92	0.01	0.01	0.08	0.07	0.79	0.56	0.89	0.11	0.36
60	-0.01	-0.08	-0.01	0.27	0.16	0.05	0.05	0.10	0.01	0.10	0.57	1.04	0.25	0.50

(a) *pointy_nose*

iter	mouth_slightly_open	big_nose	male	bushy_eyebrows	arched_eyebrows	smiling	high_cheekbones	pointy_nose	wearing_lipstick	heavy_makeup	oval_face	attractive	young	Coefficient
0	-0.05	-0.86	-0.00	0.08	-0.01	0.29	0.28	1.00	0.00	0.03	0.10	0.49	-0.00	0.00
5	-0.05	-0.86	-0.00	0.08	-0.01	0.29	0.28	1.00	0.00	0.03	0.10	0.49	-0.00	0.00
10	-0.05	-0.86	-0.00	0.08	-0.01	0.29	0.29	1.00	0.00	0.03	0.10	0.49	-0.00	0.01
15	-0.05	-0.86	-0.00	0.08	-0.01	0.30	0.29	1.01	0.00	0.02	0.10	0.49	-0.01	0.01
20	-0.05	-0.86	-0.00	0.08	-0.01	0.30	0.30	1.02	0.00	0.02	0.10	0.49	-0.01	0.02
25	-0.05	-0.85	-0.00	0.08	-0.01	0.30	0.32	1.03	0.00	0.02	0.09	0.48	-0.02	0.03
30	-0.05	-0.84	-0.00	0.08	-0.01	0.31	0.34	1.05	0.00	0.02	0.09	0.47	-0.03	0.05
35	-0.06	-0.82	-0.00	0.08	-0.01	0.33	0.40	1.07	0.00	0.02	0.09	0.46	-0.04	0.09
40	-0.07	-0.78	-0.00	0.08	-0.00	0.35	0.47	1.10	0.00	0.02	0.09	0.42	-0.06	0.13
45	-0.07	-0.66	-0.00	0.09	-0.00	0.37	0.54	1.14	0.00	0.01	0.07	0.32	-0.09	0.21
50	-0.07	-0.34	-0.00	0.09	0.00	0.37	0.62	1.11	0.00	0.00	0.02	0.13	-0.11	0.32
55	-0.07	0.11	0.00	0.09	0.01	0.38	0.69	0.94	-0.00	-0.01	-0.07	-0.13	-0.12	0.50
60	-0.07	0.11	0.00	0.09	0.01	0.38	0.69	0.94	-0.00	-0.01	-0.07	-0.13	-0.12	0.50

iter	mouth_slightly_open	big_nose	male	bushy_eyebrows	arched_eyebrows	smiling	high_cheekbones	pointy_nose	wearing_lipstick	heavy_makeup	oval_face	attractive	young	Coefficient
0	0.33	0.25	-0.00	-0.00	0.05	1.00	0.90	0.02	0.00	0.01	0.12	0.13	-0.27	0.00
5	0.33	0.23	-0.00	-0.00	0.04	1.00	0.90	0.02	0.00	0.01	0.12	0.14	-0.27	-0.00
10	0.33	0.23	-0.00	-0.00	0.04	1.00	0.90	0.02	0.00	0.01	0.12	0.14	-0.27	-0.00
15	0.34	0.21	-0.00	-0.00	0.04	1.00	0.89	0.02	0.00	0.01	0.13	0.15	-0.26	-0.00
20	0.35	0.18	-0.00	-0.00	0.02	1.00	0.88	0.02	0.00	0.01	0.14	0.17	-0.25	-0.00
25	0.36	0.14	-0.00	-0.00	-0.01	1.00	0.86	0.02	0.00	0.01	0.15	0.21	-0.22	-0.01
30	0.39	0.08	-0.00	-0.00	-0.04	1.00	0.83	0.02	0.01	0.01	0.17	0.27	-0.19	-0.01
35	0.44	-0.01	-0.00	0.00	-0.08	1.00	0.79	0.02	0.01	0.02	0.19	0.35	-0.13	-0.01
40	0.51	-0.14	-0.00	0.00	-0.14	1.00	0.76	0.02	0.01	0.03	0.24	0.49	-0.04	-0.02
45	0.63	-0.29	-0.00	0.00	-0.21	0.99	0.68	0.02	0.01	0.05	0.27	0.64	0.09	-0.03
50	0.85	-0.58	-0.00	0.00	-0.35	0.97	0.60	0.02	0.02	0.10	0.41	1.02	0.34	-0.05
55	1.38	-1.51	-0.01	0.01	-0.80	0.88	0.51	0.04	0.04	0.24	0.91	2.34	1.22	-0.08

(b) *smiling*

iter	mouth_slightly_open	big_nose	male	bushy_eyebrows	arched_eyebrows	smiling	high_cheekbones	pointy_nose	wearing_lipstick	heavy_makeup	oval_face	attractive	young	Coefficient
0	-0.04	-0.49	-0.08	0.20	0.08	0.09	-0.09	0.22	0.29	1.04	0.67	1.00	0.24	0.00
5	-0.04	-0.49	-0.08	0.20	0.08	0.09	-0.09	0.22	0.29	1.04	0.67	1.00	0.24	0.00
10	-0.04	-0.49	-0.08	0.20	0.08	0.09	-0.09	0.22	0.29	1.04	0.67	1.00	0.24	0.00
15	-0.04	-0.49	-0.08	0.20	0.08	0.09	-0.09	0.22	0.29	1.05	0.67	1.00	0.24	0.01
20	-0.04	-0.49	-0.08	0.20	0.08	0.09	-0.09	0.22	0.29	1.05	0.67	1.01	0.24	0.02
25	-0.04	-0.49	-0.08	0.20	0.08	0.09	-0.09	0.22	0.30	1.06	0.68	1.01	0.24	0.03
30	-0.04	-0.49	-0.08	0.21	0.08	0.09	-0.09	0.22	0.30	1.06	0.68	1.02	0.24	0.05
35	-0.05	-0.57	-0.12	0.30	0.13	0.10	-0.10	0.26	0.41	1.15	0.71	1.04	0.37	0.07
40	-0.05	-0.57	-0.12	0.31	0.13	0.10	-0.10	0.26	0.41	1.18	0.73	1.07	0.37	0.12
45	-0.05	-0.58	-0.12	0.32	0.13	0.10	-0.10	0.26	0.42	1.21	0.75	1.09	0.37	0.17
50	-0.05	-0.79	-0.89	0.96	0.69	0.14	-0.13	0.43	1.20	1.45	0.87	1.20	1.11	0.26
55	-0.03	-0.85	-1.15	1.22	0.98	0.17	-0.12	0.49	1.38	1.58	0.97	1.31	1.33	0.36
60	-0.13	-0.80	-0.88	1.11	0.76	0.16	-0.14	0.46	1.34	1.70	1.00	1.40	1.19	0.50

(c) *attractive*

Figure 11: Visualization of the training from §A.1 reducing the bias of *big_nose*. The model being evaluated is $f'_{target}(x) = f_{target}(x) + \beta f_{big_nose}(x)$ where β is specified by the coefficient column. The metric here is relative change computed between the $f'_{target}(x)$, where *target* is specified in the caption, and the classifier specified by the column header. The top row is from the training set performed on batches (which explains the variance) and the second row is the results on the entire validation set. The row of each table is for a specific iteration. The iterations proceed downward. The training of *attractive* shown here does not result in a debiased model, the relative change diverges from 0 indicating a failed training.